Chapter 3

Numerical Modelling

3.1 General Discussion

CBM walls are inherently composite in nature and exhibits non-linear behaviour. Therefore, many experimental studies have been carried out in the past to capture its non-linear behaviour for in-plane or out-of-plane loads [37], [79]–[81]. Experimental tests have proved to be instrumental for better understanding this unconventional construction method's capacity, failure modes, and energy dissipation [33], [82], [83]. Although such tests have been insightful in understanding the response of CBM structures, carrying out parametric experimental studies can be costly and time-consuming [75]–[77]. On the other hand, advances in numerical modelling techniques like the finite element (FE) method have proved to be an alternate efficient, robust and less expensive technique for understanding CBM structures. A numerical modelling technique can be used, if not to replace the experimental tests, to complement them and, to substitute the economic resources with the computational resources [84]. By employing numerical techniques, it is possible to comprehensively assess the impact of a wide range of geometrical configurations on the response of CBM structures. These configurations include variations in opening sizes, their positions within the structure, different aspect ratios, and the presence of slender or short walls. Additionally, the analysis can extend to examining the influence of different material properties, such as masonry unit types and mortar mix compositions, allowing for a more thorough understanding of how these factors

contribute to the overall structural behaviour under various loading conditions [78].

Designers and researchers require reliable and efficient numerical methods capable of accurately predicting the response of CBM structures. These methods are essential for assessing future advancements in design and rehabilitation strategies, enabling the development of more resilient and optimised CBM buildings. Accurate numerical predictions are crucial for evaluating the structural performance under various loading conditions, ensuring that new designs and rehabilitation approaches can meet the demands of safety, durability, and seismic resilience. Several authors [85], [86] have proposed a diverse array of modelling techniques, each offering different levels of accuracy and computational efficiency. These methods range from simplified approaches that prioritise speed and ease of use to more complex models that provide a higher degree of precision but require significantly more computational resources. The choice of technique often depends on the specific requirements of the study, such as the desired balance between accuracy and computational time, as well as the complexity of the structural behaviour being investigated. Three types of numerical models have been used to simulate masonry: a) micro-models, b) macro-models, and c) simplified micro-models.

In the micro-modelling technique (Figure 3.1a), the unit and mortar of a CBM structure are modelled separately and the interface between them is defined based on the contact conditions. The inelastic properties and elastic (Young's modulus, Poisson's ratio, and compressive strength) properties of both the unit and mortar are individually considered. The micro-modelling approach has been successfully implemented to study the behaviour of unconfined masonry in small assemblages as well as larger structures [87]–[89]. Micro-modelling with the discrete element method (DEM) which remarkably reflects the structure of masonry in its natural state, where bodies can interact, separate, and influence one another has been used for confined brick masonry [90]. Despite its high accuracy, this approach is prohibitively computationally expensive, often making it unsuitable for designers and engineers.

The macro-modelling technique as shown in Figure 3.1b, do not differentiate between units, mortar joints, and their interfaces; therefore, they are not modelled separately. Using homogenisation techniques, the material properties of the entire masonry wall is characterised

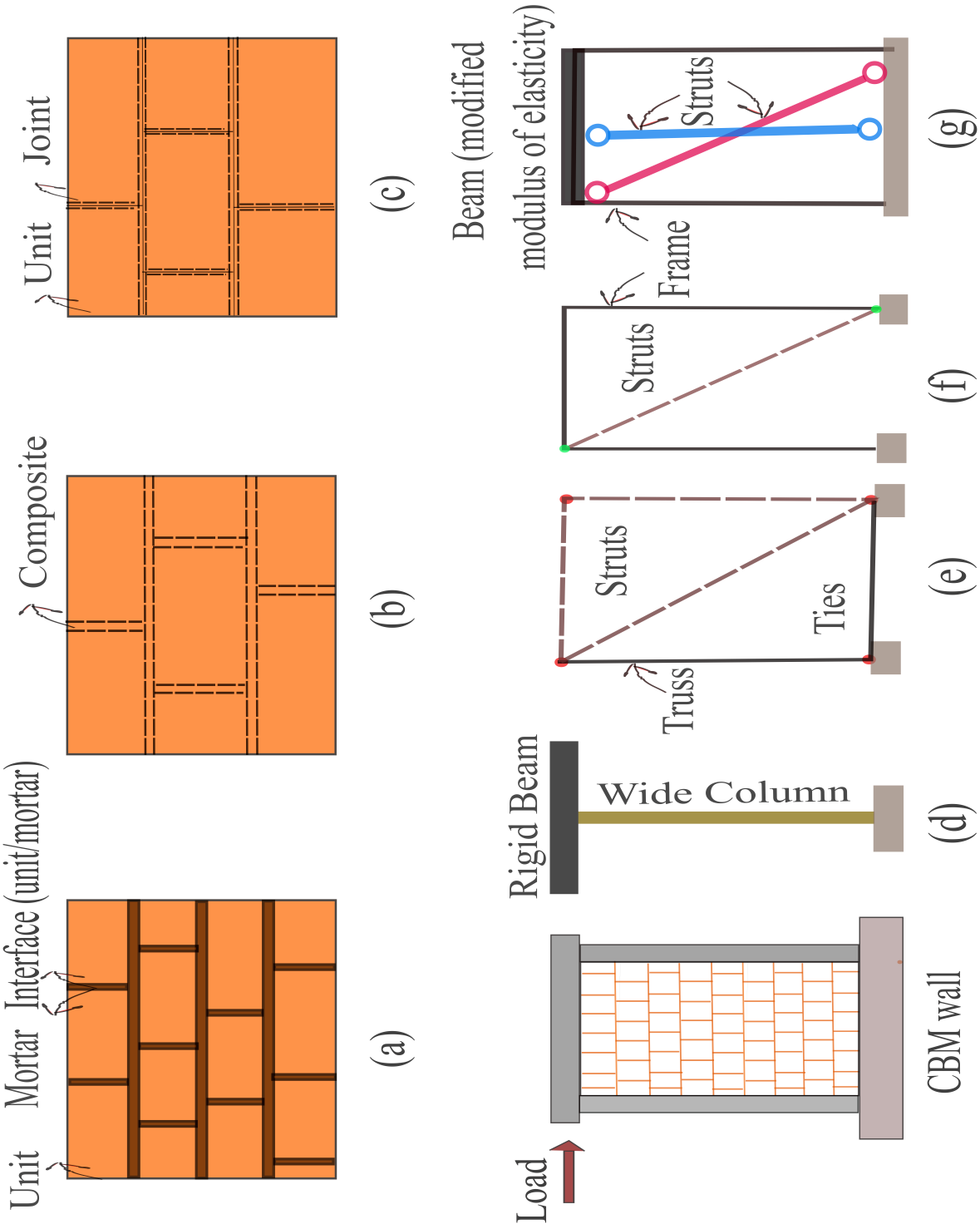

Figure 3.1: Modelling strategies for CBM structures: (a) Micro model; (b) macro model; (c) Simplified micro model; (d) WCM; (e) STM; (f) ESM; (g) V-D strut

as homogenised material [67]–[69]. Okail et al. [59], Tripathy and Singhal [45], Borah et al. [34] and Acharya et al. [91] adopted macro-modelling approach to avoid defining each brick, mortar, and interface's input properties individually and to simulate the non-linear behaviour of CBM walls. For the same continuum elements have been used to model masonry panels and RC elements. The contact between them has been simulated by specifying appropriate contact parameters such as hard contact in normal direction and frictional contact in tangential direction. Medeiros et al. [73], adopted a smeared crack model for modelling crack propagation in the masonry and RC elements. Eshghi and Pourazin [8] developed a 2-D macro model for CBM walls that combined a coulomb-friction model with a tension cut-off mode for the interface zone between the constraining elements and the masonry panel with plasticity-based material models.

In the simplified micro-modelling technique as shown in Figure 3.1c, each joint containing mortar and the two unit-mortar interfaces is bunched into an average interface, while the units are allowed to expand in both directions. As a result, this method provides a coarse but less computationally demanding alternative to micro-modelling. When an intermediate level of fineness and accuracy is needed, this approach is thought to be a suitable alternative to coarse modelling strategies [59], [92].

The accuracy of analysis results tends to diminish as the modelling approach shifts from a micro-level focus, which deals with detailed and specific elements, to a macro-level focus, which encompasses broader and more generalised aspects [93]. This reduction in precision occurs because micro-modelling captures finer details and interactions, while macro-modelling abstracts and simplifies these complexities for a wider perspective.

Aside from the methods outlined above, several further simplified models have been developed to simulate the behaviour of CBM walls with a reasonable amount of accuracy. The Wide Column Model (WCM) is one of the most widely investigated macro-modelling technique used for linear elastic analysis of CBM structures that idealises a multi-story wall and slab structure as an analogous moment-resisting frame as shown in Figure 3.1d [94]. While WCM is suitable for modelling the overall behaviour of CBM walls, it is unable to depict the

interaction at the interface between the masonry and the RC tie column and stress concentrations around the openings. The linear models of WCM have been also extended by Gilmore et al. [95] to consider geometric non-linearity allowing large deformations.

Apart from WCM, strut and tie model (STM) has been also extensively used as a modelling method for CBM structures. In STM, a structure subjected to lateral loads is represented using a truss-like system, i.e., the tensile stress path (ties) is interconnected to the compressive stress path (struts) as shown in Figure 3.1e. If the STM is statically determinate the design member force is derived using static equilibrium [96], [97].

The equivalent strut model (ESM) is another modelling technique for RC buildings with masonry infill, which has been further developed for CBM structures. In ESM, the lateral load resistance of masonry walls is defined by a diagonally placed strut with a released end moment as shown in Figure 3.1f. To simulate the behaviour of CBM walls using ESM, Torrisi et al. [98] presented different models with struts positioned diagonally. The V-D strut model was introduced by Borah et al. [99] is an improved version of the existing ESM technique which in addition to the diagonal strut, also modelled a vertical strut, to simulate realistic tie-beam axial forces and tie-beam deflection as shown in Figure 3.1g.

Although the aforementioned modelling approaches have been used in predicting the behaviour of CBM structure, all of them manifest their own limitation. In the case of the STM and ESM approach, the failure of tie columns is difficult to predict as both of these approaches do not consider the non-linearity of tie members. The WCM approach does not take into account the individual behaviour of tie-column members of the structure. In FEM, the macro-model technique discussed earlier simulates the interfaces using the traction separation law with frictional properties assigned in the tangential direction and hard contact in the normal direction, which leads to a complex modelling approach and computationally demanding simulation. In this work, a macro-model has been employed that did not account for the masonry tie contact individually. This is supported by the fact that concrete and masonry work monotonically during a seismic event, which has been proved by many authors that have carried out experimental campaigns. Consequently, we have developed a computa-

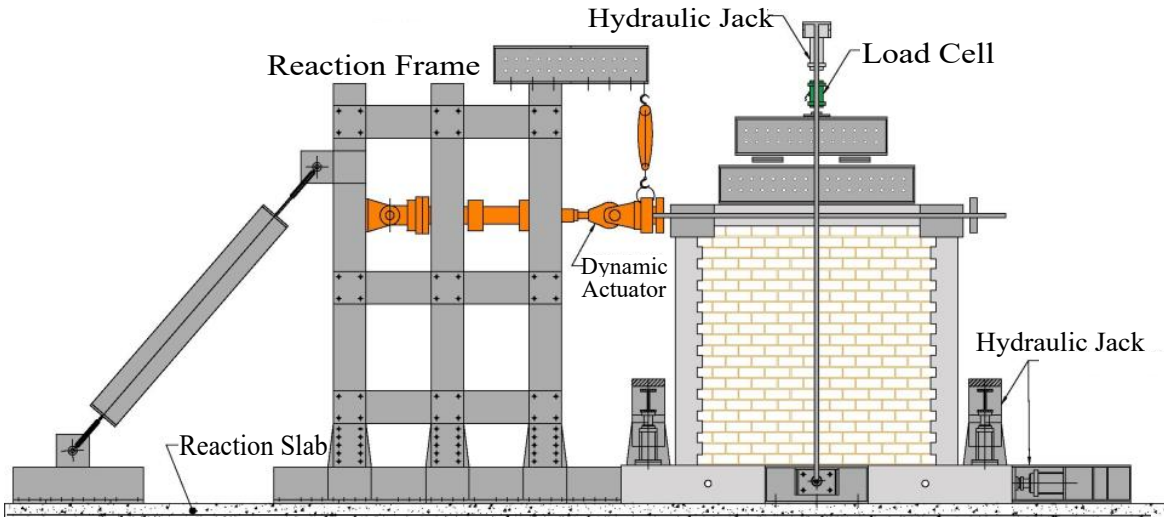

Figure 3.2: Typical assemblage with test setup

tional less expensive model which is able to undertake several parametric studies with varied geometrical configurations and materials to explore the individual behaviour of CBM systems. In this research, a macro model approach is employed, treating masonry and RC tie contacts as a single monolithic structural element. This is based on the understanding that concrete and masonry work monolithically during seismic events, as demonstrated in earlier experimental studies [100], [101]. This approach allows for an extensive parametric study with varied geometrical and material properties to explore the behaviour of CBM systems at a low computational cost.

3.2 Finite element modelling

To predict the lateral capacity of CBM structures, a FE model of CBM walls is developed using ABAQUS [102]. A three-dimensional non-linear FE model has been developed to grasp the main components of the CBM structural system. The developed numerical modelling procedure is based on the FE models described in Jhair et al. [72] which attempts to simulate the experiments conducted by Machengo & Pari [103]. Figure 3.2 shows this typical assemblage with the test set-up used in the FE model. A comprehensive macro-modelling strategy is developed, where the wall and foundation are considered as a single, integrated unit. This approach assumes monolithic behaviour at each point of contact between different materials, which is consistent with the construction techniques used in CBM structures

[72], [100], [104], [105]. In this method, the masonry wall panel and the confining columns are connected using a toothed connection, which ensures a seamless interaction between the components, promoting monolithic behaviour throughout the structure.

By employing the macro-modelling technique, the various elements involved—such as the brick masonry, mortar joints, and concrete components—are all simulated as cohesive parts of the system. The corresponding interfaces between these materials are also incorporated into the model, allowing for an accurate representation of the structural behaviour under different conditions. This strategy enables a detailed analysis of the interactions between the different materials and components, providing insights into the overall performance of the CBM system under various loading scenarios .

Three-dimensional solid finite element models offer the most accurate representation of structural behaviour under complex loading conditions [106]. Therefore, a 8-noded solid continuum three-dimensional element, C3D8R, is used to model concrete and brick masonry. The reinforcement bars are modelled as trusses using 3D elements (T3D2) with two nodes per element. Perfect adhesion (no-slip condition) is considered through an embedded constraint using the interaction module of ABAQUS. As a boundary condition, the reaction slab over which the CBM wall is placed (as illustrated in Figure 3.2) is modelled as an analytical rigid surface. Together with the dynamic actuator, the hydraulic jack frame and reaction are modelled as analytical rigid surfaces in order to prevent the foundation from sliding horizontally. The hydraulic jacks are designed to keep the foundation from toppling and are modelled as pin supports with just the vertical component constrained. For this purpose, it is assumed that there is a 2:1 slope in the pressure transmission between these reaction slabs and the hydraulic jacks [103]. Figure 3.3 depicts a simplified diagram of the FE model developed from the experimental test setup (Figure 3.2) of the CBM wall with FE elements, loading and boundary conditions.

The discrete crack model and the smeared crack model are two techniques that are extensively used in the FE framework for modelling of concrete cracking [107]. A crack is treated as a geometrical identity in the discrete model, so it is either already embedded in the FE

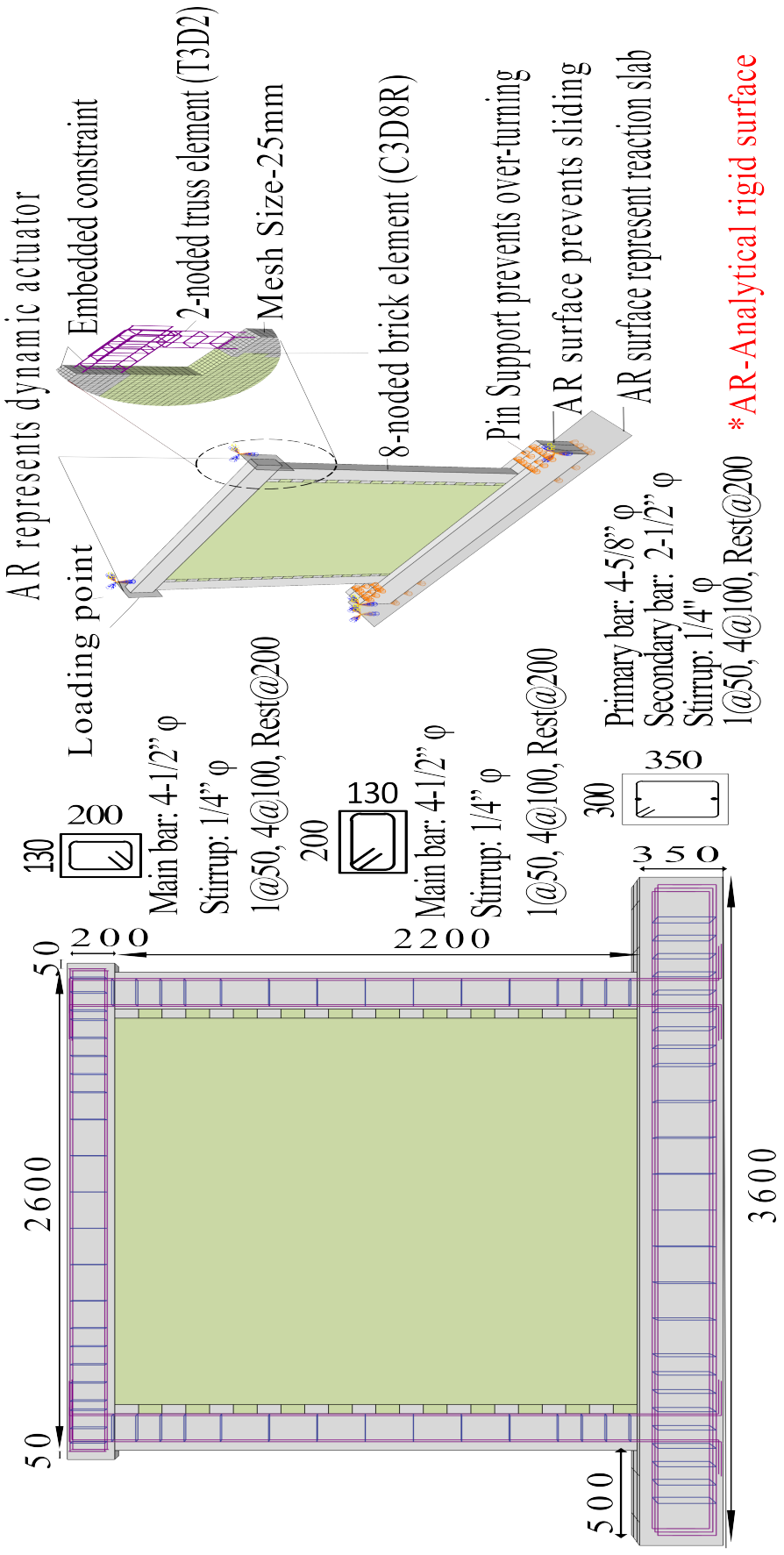

Figure 3.3: A simplified diagram of the FE model of CBM wall showing elements, loading, boundary conditions and mesh size

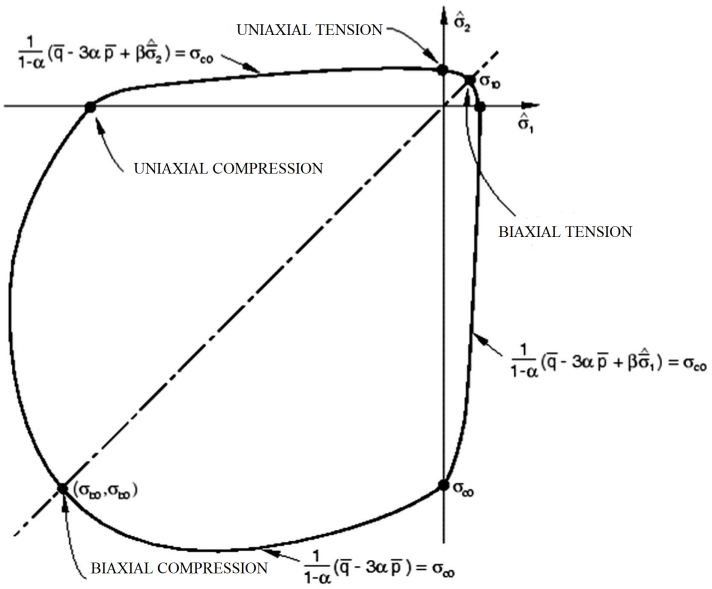

Figure 3.4: Failure (Yield) surface of CDP in plane stress [72]

mesh [108] or by repeated meshing [109]. The latter maintains the geometry (and thus the mesh) unchanged, and the concrete constitutive law replicate crack formation and propagation [107].

A variant of classical plasticity theory with the introduction of damage concepts is commonly used with Concrete Damage Plasticity (CDP) to simulate the non-linear behaviour of quasi-brittle materials. However, its accuracy remains questionable due to limitations in its tensile behaviour formulation [110]. Even when tensile stiffness degradation is accurately simulated, as demonstrated by experimental tensile cyclic tests [111], the formulation may fail under strong excursions between tensile and compressive strains. Since the primary objective of the present thesis is to assess the seismic performance of confined brick masonry (CBM) structures, including the capacity curves of walls, pushover analyses were employed. This approach was designed to minimise severe transitions between tensile and compressive strains, ensuring more reliable performance predictions. In the following subsection, Concrete Damage Plasticity (CDP) model is discussed.

3.2.1 Concrete Damage plasticity

The Concrete Damaged Plasticity (CDP) model is a widely used computational technique in mechanics, particularly for simulating the behaviour of concrete structures subjected to vari-

ous stress conditions. This model helps predict the two main failure mechanisms in concrete: crushing of the material under compressive stress and cracking under tensile stress. The evolution of the failure surface in the CDP model is governed by two hardening variables, which are associated with these distinct failure modes—compression and tension. These variables control how the yield (or failure) surface develops and responds to the applied loads, ensuring that the model accurately captures the concrete's failure behaviour under different loading conditions.

Yield surface: The yield surface shows the critical stress state, which is the level of stress above which plastic deformation should start. The yield function, F, of the CDP model is generally defined in terms of effective stresses as illustrated in Figure 3.4 and takes the following form,

$$
\begin{aligned}
&F = \frac{1}{1-\alpha}\left(\bar{q} - 3\alpha\bar{p} + \beta\left(\tilde{\varepsilon}^{pl}\right)\left\langle\hat{\bar{\sigma}}_{\max}\right\rangle - \gamma\left\langle-\hat{\bar{\sigma}}_{\max}\right\rangle\right) - \bar{\sigma}_c\left(\tilde{\varepsilon}_c^{pl}\right) \leqslant 0 \\
&where, \\
&\alpha = \frac{(\sigma_{bo}/\sigma_{co}) - 1}{2\,(\sigma_{bo}/\sigma_{co}) - 1}; 0 \leqslant \alpha \leqslant 0.5 \\
&\beta\left(\tilde{\varepsilon}^{pl}\right) = \bar{\sigma}_c\left(\tilde{\varepsilon}_c^{pl}\right)/\bar{\sigma}_t\left(\tilde{\varepsilon}_t^{pl}\right)(1-\alpha) - (1+\alpha) \\
&\gamma = 3\,(1-K_c)\,/2K_c - 1
\end{aligned}
\tag{3.1}
$$

where, $\bar{q}$ is the Von-Mises equivalent effective stress, $\bar{p}$ is the hydrostatic pressure stress, $\hat{\bar{\sigma}}_{\max}$ is the maximum principal effective stress, σ_{bo}/σ_{co} is the ratio of initial bi-axial compressive yield stress to initial uni-axial compressive yield stress, K_c is the ratio of the tensile meridian to the compressive meridian and also defines the yield surface's appearance in the deviatory plane, $\bar{\sigma}_c$ and $\bar{\sigma}_t$ are the respective compressive and tensile effective stress and $\tilde{\varepsilon}_c^{pl}$ and $\tilde{\varepsilon}_t^{pl}$ are the respective compressive and tensile equivalent plastic strains.

Non-associated flow: The CDP model assumes the following non-associated potential flow

$$
\dot{\varepsilon}^{pl} = \dot{\lambda}\frac{\partial G(\bar{\sigma})}{\partial\bar{\sigma}} \tag{3.2}
$$

Table 3.1: Parameters used to define concrete damage parameters [72]

Parameters	**Values**
Expansion angle of the concrete	30
Expansion angle of the masonry	35
Eccentricity e	0.01
σ_{b0}/σ_{c0}	1.16
K_c	$2/3$
Viscosity parameter	0.0001

For this model, the Drucker-Prager hyperbolic function with the following definition is chosen as the flow potential 'G':

$$G(\sigma) = \sqrt{(e\sigma_{to}\tan\psi)^2 + \bar{q}^2} - \bar{p}\tan\psi \tag{3.3}$$

where σ_{to} is the uniaxial tensile stress at failure, e is the eccentricity that gives the rate at which the plastic potential function approximates the asymptote, and ψ is the dilation angle measured at high confining pressure and is an indicator of the direction of the plastic strain increment.

The essential parameters required for CDP are taken from the characterisation of uniaxial, biaxial, and triaxial test data outlined in Jankowiak and Lodygowski [112]. The parameters required for the CDP model in ABAQUS include the dilation angle ψ, eccentricity e, the ratio of biaxial to uniaxial compressive yield stresses σ_{b0}/σ_{c0}, the ratio of the second stress invariant on the tensile meridian to that on the compressive meridian K_c, and the viscosity parameter μ. For the dilation angle ψ, values of 30° and 35° were used for concrete and masonry, respectively, as correctly applied by Breveglieri et al. [80]. In the absence of experimental results, the remaining parameter values were taken as Table 3.1. These values show good results when modelling quasi-brittle materials with the CDP model, as evidenced by the work of D'Altri et al. [113] , Nasiri and Liu [114], Breveglieri et al. [80], Bolhassani et al. [69], Szczecina and Winnicki [115], among others. It is important to note that these parameter values are specific to the referenced study and may vary depending on the material and application under investigation.

Table 3.2: Adopted mechanical properties of materials as component of CBM structures [72]

Material	E (MPa)	ν	f'_{cm} (MPa)	f_y (MPa)	G_{ch} (N/mm)	G_f (N/mm)
Foundation Concrete	25900	0.15	27.5	2.75	13.7	0.137
Column Concrete	21300	0.15	16.5	1.95	8.60	0.12
Top Beam Concrete	27500	0.15	31.50	3	14.9	0.136
Masonry	5700	0.15	10	1.40	-	0.12
Steel rebars	200000	0.3	-	420	-	-

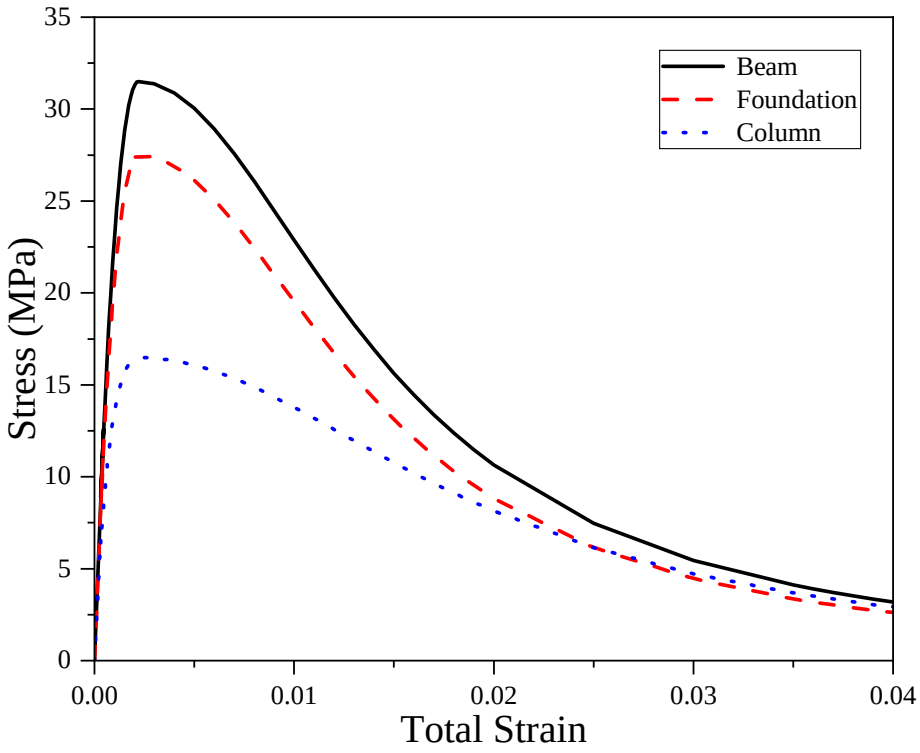

Figure 3.5: Stress-Strain relation of concrete in compression [72]

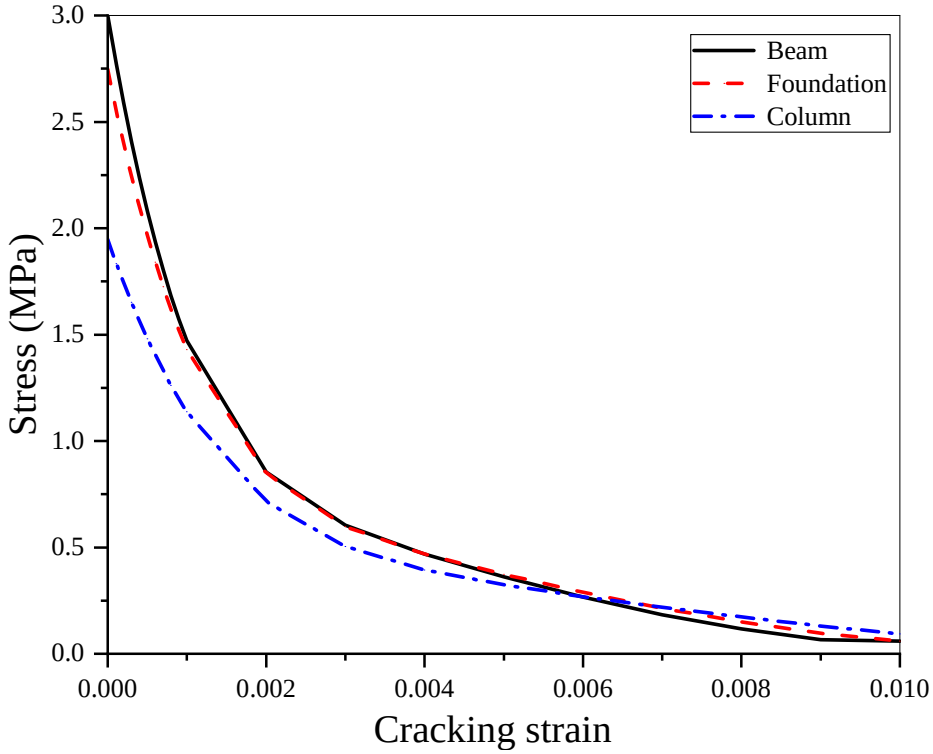

Figure 3.6: Stress-Strain relation of concrete in tension [72])

3.2.2 Material and Damage Modelling

The material properties for all components of the wall used for modelling purpose has been shown in the Table 3.2 where ν is the poisson's ratio, E is Young's modulus, $f_{cm}^{'}$ is the compressive strength & f_y is the tensile strength, G_{ch} is the crushing energy and G_f is the fracture energy of the materials. It is well known that the behaviour of concrete and masonry falls between ideal brittle and ductile in terms of their constitutive laws. They both qualify as quasi-brittle materials because their behaviour is more brittle than ductile [116]. The constitutive models and damage models for concrete, masonry, and steel reinforcement has been discussed below.

Concrete:

As shown in Figure 3.5, three major components namely linear, hardening, and softening are used to describe the compressive behaviour of concrete. The linear portion is used up to a compressive stress of 0.4 $f_{cm}^{'}$. According to CEB-FIP [117], parabolic hardening characterised the second part up to the peak strength $f_{cm}^{'}$ and its corresponding strain ϵ_{cm}. The final section is interpreted as a softening of the hyperbola according to Krätzig and Pölling [118].

$$\sigma_{c(1)} = E_0 \varepsilon_c$$
$$\sigma_{c(2)} = \frac{E_{ci}\frac{\varepsilon_c}{f_{cm}} - \left(\frac{\varepsilon_c}{\varepsilon_{cm}}\right)^2}{1 + \left(E_{ci}\frac{\varepsilon_{cm}}{f_{cm}} - 2\right)\frac{\varepsilon_c}{\varepsilon_{cm}}} f_{cm}$$
$$\sigma_{c(3)} = \left(\frac{2 + \gamma_c f_{cm} \varepsilon_{cm}}{2 f_{cm}} - \gamma_c \varepsilon_c + \frac{\varepsilon_c^2 \gamma_c}{2\varepsilon_{cm}}\right)^{-1}$$

where

$$\gamma_c = \frac{\pi^2 f_{cm} \varepsilon_{cm}}{2\left[\frac{G_{ch}}{l_{eq}} - 0.5 f_{cm}\left(\varepsilon_{cm}(1-b) + b\frac{f_{cm}}{E_0}\right)\right]^2}$$

According to the CEB-FIP model code [117], the relevant parameters are expressed as $\varepsilon_{\text{cm}} = 0.0022$, $f_{cm} = f_{ck} + 8$, where f_{ck} is the characteristic compressive strength. The modulus of elasticity E is given by $E_{ci} = 10000 f_{cm}^{1/3}$ and $E_0 = (0.8 + 0.2 f_{cm}/88) \times E_{ci}$, where E_0 is the secant modulus corresponding to a stress of $0.4 f_{cm}$. Both stress and modulus of elasticity are expressed in MPa. The crushing energy per unit area, G_{ch} is measured in Nmm/mm^2. The characteristic length l_{eq} is determined by the mesh size, element type, and crack direction [119]. In this study, l_{eq} is considered equal to the mesh size to account for the expected crack direction in the concrete. Finally, the parameter is determined by averaging the ratio $\epsilon_{pl}/\epsilon_{ch}$ over the relevant strain range. Initially, = 0.70 is assumed, but this value is iterated until convergence is achieved. Figure 3.5 presents the stress-strain curves used for concrete in compression.

Further, the tensile behaviour is assumed to be controlled firstly by a linear elastic component up to its tensile strength, after which tensile failure sets in. The formulation provided by Hordijk [120] is used to define the post-failure behaviour of cracked concrete in strain-softening terms as given by-

$$\begin{aligned} \sigma_{t(1)} &= E_0 \varepsilon_t \\ \frac{\sigma_{t(2)}}{f_{tm}} &= \left[1 + \left(c_1 \frac{w}{w_c}\right)^3\right] e^{-c_2 \frac{w}{w_c}} - \frac{w}{w_c}\left(1 + c_1^3\right) e^{-c_2} \end{aligned} \tag{3.4}$$

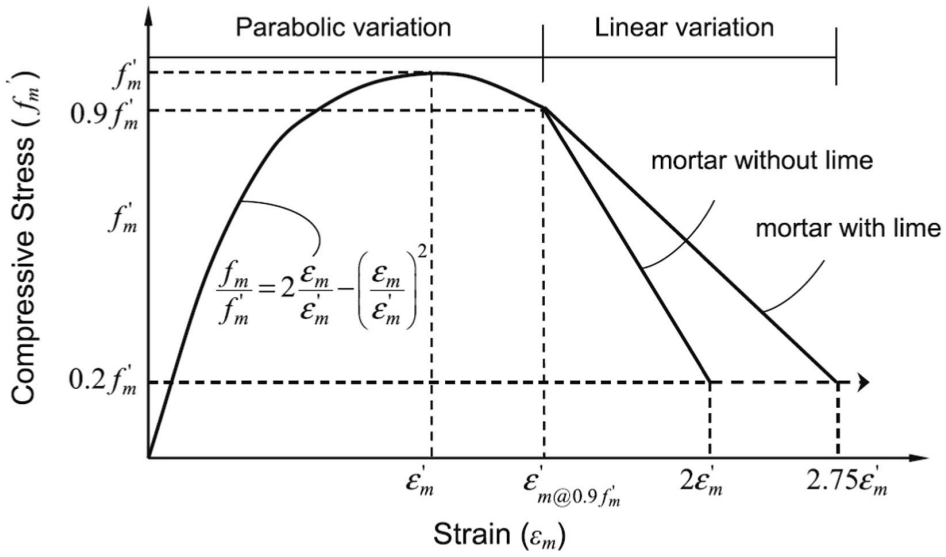

Figure 3.7: Stress-Strain formulation for masonry in compression [121]

where, c_1=3, and c_2=6.93 [120], w_c is the critical crack opening at which the tensile stress σ_t becomes zero. This is calculated using $w_c = 5.14/\left(G_f f_{tm}\right)$. Additionally, in the absence of experimental data, the fracture G_f is estimated as $G_f = 0.073 \times \left(f_{cm}\right)^{0.18}$ [117]. Similarly, the crushing energy G_{ch} is estimated as $G_{ch} = \left(f_{cm}/f_{tm}\right)^2 \times G_f$ [122]. It is important to note Equation 3.4 defines the post-failure tensile behaviour in terms of crack opening w (mm). However, for reinforced concrete, the post-failure relationship is typically expressed in terms of strains to prevent the results from being dependent on the mesh size. Therefore, the cracking strain is expressed as $\epsilon_{ck} = w_c/l_{eq}$. Figure 3.6 illustrates the adopted post-failure stress-strain curves for the tensile behaviour of concrete. It should also be noted that a residual stress $\sigma_r = f_{tm}/50$ is used to prevent kinetic instabilities.

Masonry:

According to the constitutive model proposed by Kaushik et al. [121], the compressive behaviour of masonry comprises three main components: (1) parabolic hardening, (2) linear softening, and (3) residual stress, as shown in Figure 3.8. In this study, a residual stress of 0.1 $f_{cm}^{'}$ have been adopted, rather than 0.2 $f_{cm}^{'}$, to prevent kinetic instabilities, following the recommendations of Lourencco [92], as illustrated in Figure 3.8.

Similar to concrete, tensile behaviour of masonry begins with linear elasticity followed by non-linear behaviour, which assumes exponential softening post-failure [92]. It is important

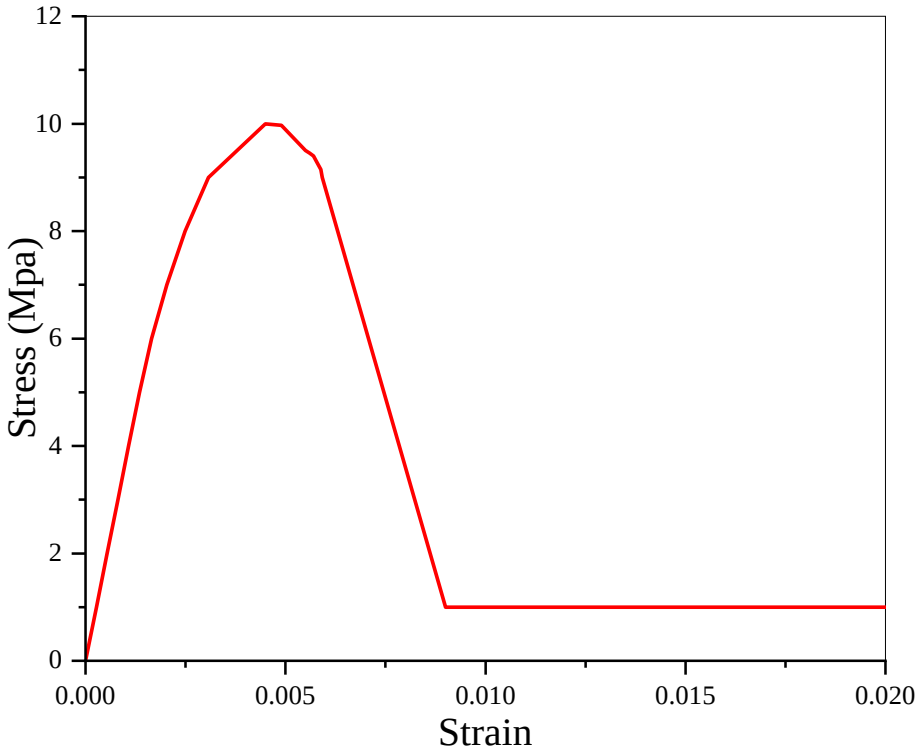

Figure 3.8: Constitutive laws for masonry in compression [72]

to remember that the masonry panel does not have reinforcement, unlike reinforced concrete, which might cause the results to be too sensitive to mesh when a post-failure stress-strain curve is defined [102]. Hillerborg et al. [123] fracture energy proposal is used to define a post-failure stress-displacement curve to resolve this issue, Equation 3.5. The adopted stress-strain curves for the masonry in compression and tension is shown in Figure 3.9.

$$\begin{aligned} \sigma_{t(1)} &= E_0 \varepsilon_t \\ \sigma_{t(2)} &= f_{tm} \exp\left(-\frac{f_{tm} w}{G_f}\right) \end{aligned} \tag{3.5}$$

Steel reinforcement:

In scenarios where the predominant factor is the behaviour of reinforced concrete, it is imperative to give due consideration to the phenomenon of bond slip that occurs between the steel reinforcement and the concrete. The term ”bond-slip” is the mechanical contact between a steel reinforcing bar and the concrete around it. This allows transferring tensile stress from steel to concrete. It is the mechanism that anchors straight reinforcing bars. It influences

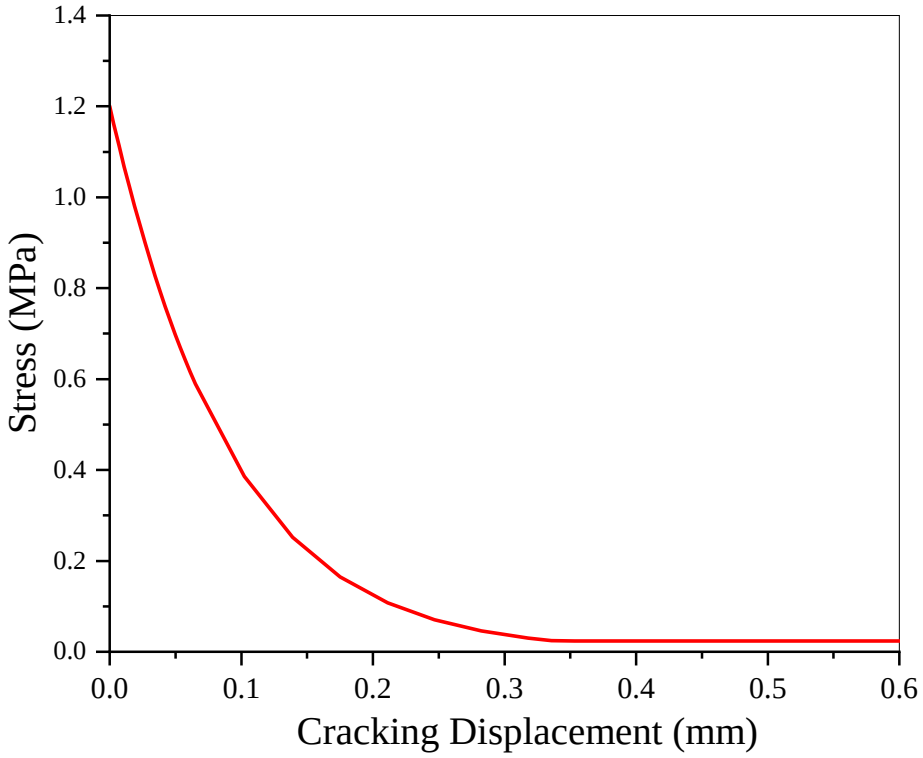

Figure 3.9: Constitutive laws for masonry in tension [72]

many other key features of structural concrete such as crack control and section stiffness [124]. In CBM walls, where the masonry behaviour predominates, the bond-slip effect do not impact its structural behaviour. Consequently, this study does not consider this bond-slip effect.

Figure 3.10 shows the adopted constitutive stress-strain curve for steel reinforcement. The steel reinforcement is modelled as elasto-plastic material with a hardening of 2%E slope between the strains related to yield and ultimate stresses, ε_y and ε_u, respectively. In this instance, where no mechanical properties is altered, the hardening slope under consideration is derived by connecting the points associated with the established elastic limit state (ε_y,F_y) and the ultimate limit state (ε_u,F_u).

Damage model:

The damage parameters for concrete's compressive and tensile behaviour are computed following the formulation introduced by Alfarah et al. [119], a revised version of the formulation by Lee and Fenves [111]. Similarly, the pivot rule formulation proposed by Park et al [125] is employed for both compressive and tensile behaviour of masonry.

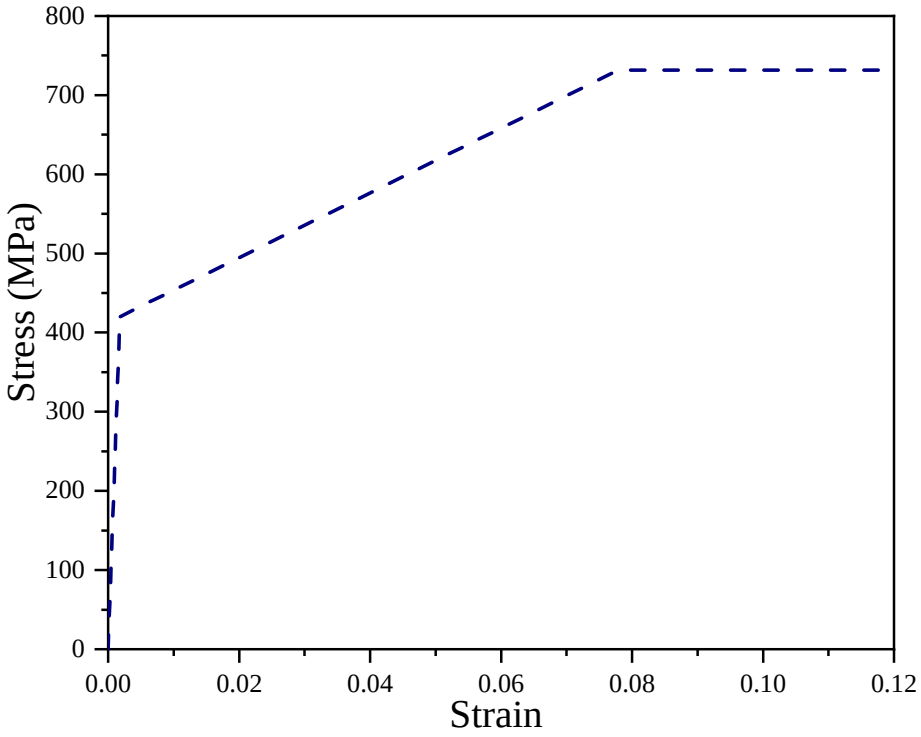

Figure 3.10: Adopted constitutive stress-strain curve for steel reinforcement [72]

It should be noted that assigning a unit value to a damage parameter signifies the complete failure of the material, implying that the material cannot sustain any additional stress. However, in the CDP formulation a unit value of the damage parameter would result in an infinite plastic strain [102]. Therefore, in the present study, all damage parameters are constrained to a maximum value of 0.98.

3.3 Pushover analysis

Pushover analysis is a highly effective method utilised in structural engineering to assess the seismic performance of buildings. This method is a static, non-linear process that estimates how structures deform when subjected to seismic forces. It is based on the concept that during an earthquake, buildings do not respond uniformly; instead, they undergo a process of internal reorganisation or ”self-redesign.” This phenomenon occurs because when one part of the building fails, the dynamic forces originally exerted on that part are transferred to other parts of the structure. Understanding and predicting these force redistribution’s are crucial for designing buildings that can withstand seismic events.

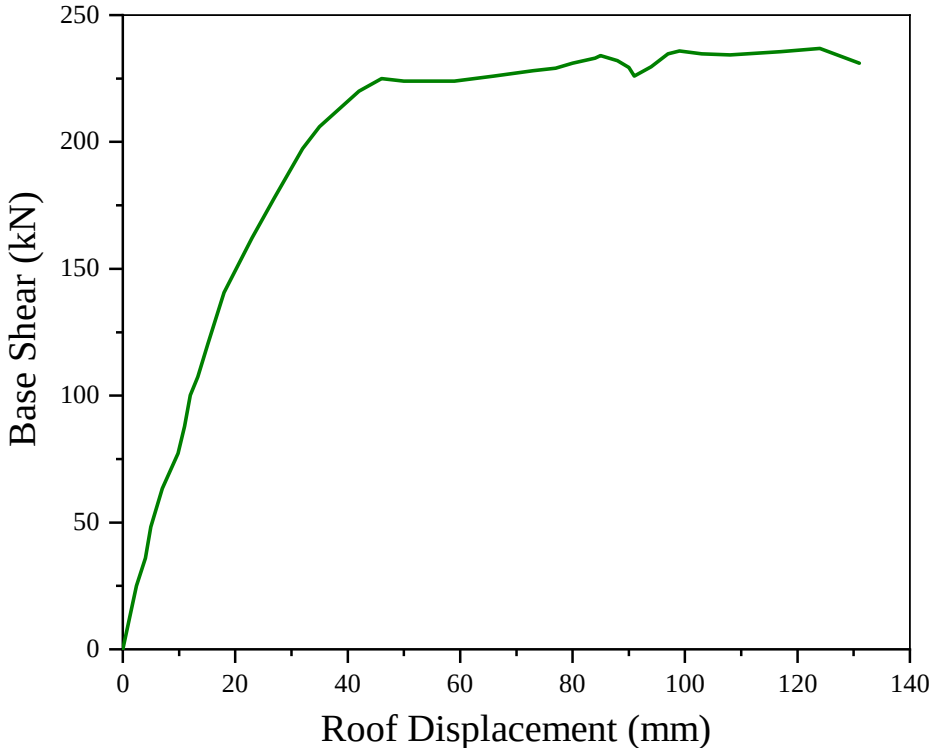

Figure 3.11: Pushover curve of structure

The pushover analysis process begins by applying gradually increasing lateral loads to the structure. These loads simulate the forces that would be experienced during an earthquake. The analysis continues until a weak point in the structure is identified. This weak point represents a location in the building that would likely experience significant damage or failure during a real seismic event. Once this weak point is located, the structural model is updated to reflect the changes brought about by this weakness. This updated model is then subjected to the same gradually increasing loads to observe how the forces redistribute in the next iteration. This iterative process continues until a predefined target lateral displacement is reached or the structure ultimately fails. Figure 3.11 shows the static pushover curve of a structure obtained from the analysis.

In this study, pushover analysis is conducted using the commercial software package ABAQUS [102]. A predefined target displacement of 20 mm is chosen as the criterion for the analysis. To minimise the impact of kinematic effects, experimental cyclic tests on walls are performed at a slow rate, simulating quasi-static conditions. Quasi-static testing is essential as it closely approximates the conditions experienced by a structure during a real earthquake, allowing

for a more accurate assessment of its seismic performance.

ABAQUS provides two robust solvers for modelling quasi-static events: the implicit solver and the explicit solver. For this research, the explicit solver is employed to model the quasi-static phenomena associated with pushover analysis. The explicit solver is chosen due to its capability to handle complex loading conditions effectively. The application of loads in the analysis is managed using smooth step amplitudes. This approach ensures that the loads are applied gradually, starting and finishing with zero velocity. Such a controlled application of loads helps to reduce the potential for kinematic effects, which could otherwise distort the results of the analysis.

To verify the quasi-static nature of the pushover analysis, the total kinetic energy (ALLKE) and the total internal energy (ALLIE) of the model are monitored throughout the entire time step. It is crucial that the kinetic energy remains less than 1% of the internal energy during the analysis. This condition ensures that the numerical results are primarily due to quasi-static effects rather than kinematic influences. By maintaining this energy ratio, the analysis can confidently attribute the observed deformations and force redistribution's to the quasi-static loading conditions, providing a reliable assessment of the structure's seismic performance. Throughout the time step, kinetic energy should amount to less than 1% of the internal energy, ensuring that kinetic effects do not affect the numerical conclusions [104], [126], [127].

Overall, pushover analysis, as conducted in this study using ABAQUS, provides valuable insights into the seismic behaviour of buildings. By understanding how structures redistribute forces and identify weak points, engineers can design more resilient buildings capable of withstanding the unpredictable and potentially devastating forces of earthquakes.

3.4 Modelling and material calibration

This section delves into the intricate process of numerical modelling for confined masonry walls, highlighting the challenges posed by the anisotropic behaviour of masonry and the need for calibrated material properties. It details the steps taken to achieve computational efficiency, accurate simulations, and alignment with experimental observations. The find-

ings underscore the critical role of tensile behaviour, along with calibrated Young's modulus, tensile strength, and fracture energy, in reproducing realistic structural responses.

Sensitivity analysis for mesh size selection

In the numerical modelling of confined masonry walls, each wall was treated as a single part. Consequently, the mesh size affected the entire model. To identify an optimal mesh size that balanced computational efficiency and accuracy, a sensitivity analysis was conducted. This analysis helped determine the most appropriate mesh size, minimising computational cost while ensuring accurate simulation results.

Experimental determination of material properties

The initial material properties of the masonry were determined experimentally through uniaxial compressive tests conducted perpendicular to the bed joints. These properties, including the Young's modulus of the masonry, are presented in Table 3.2. However, direct application of these experimentally derived properties in numerical models led to overly stiff structural responses. This observation aligns with previous findings in the literature [73]. The discrepancy arises because the macro-modelling approach simplifies the behaviour of anisotropic materials, such as masonry, into isotropic assumptions. As a result, material properties derived from small-scale specimen tests required calibration to accurately reflect the behaviour of masonry in macro-modelling.

Iterative calibration of material properties

To address these discrepancies, numerous iterations were performed by systematically varying the material properties of both the masonry and the concrete. For instance, the compressive strength of the concrete columns was adjusted, and its influence on the overall response of the wall, including cracking patterns and capacity curves, was analysed. Through these iterations, it was observed that the tensile behaviour of masonry played a pivotal role in governing the response of confined masonry walls.

Parametric study of key material properties

A subsequent parametric study focused on three critical masonry parameters: Young's mod-

ulus, tensile strength, and fracture energy. The objective was to align numerical predictions with experimental results, including load-displacement curves and observed cracking patterns. This study began with the material properties listed in Table 3.2 and systematically varied each parameter to identify optimal values.

1. Calibration of Young's modulus

The sensitivity analysis of Young's modulus revealed that an equivalent Young's modulus of E* = 65% of the initial modulus E_0, provided the best fit for the initial stiffness of the experimental results. Although variations in had minimal impact on the non-linear behaviour of the wall, the initial stiffness was found to result from the combined contributions of the concrete frames and the masonry panel. For instance, whether a value E* = 100% E_0 had been used instead of E* = 65% E_0, only a mistake of 14% would have been committed when capturing the initial experimental stiffness of the entire wall. This variation underscores the need for calibration when applying experimental values in macro-modelling.

2. Tensile strength and fracture energy

Once the Young's modulus was calibrated, attention shifted to the tensile strength of masonry (t_f) and its effect on the non-linear behaviour of the wall. Reducing the tensile strength caused earlier cracking in the masonry panel, leading to quicker degradation of stiffness. A tensile strength of 1.20 MPa was found to best replicate the experimental capacity curve's non-linear zone.

Similarly, fracture energy (G_f) was varied and lower values of fracture energy were associated with faster cracking propagation and stiffness degradation. A value of 0.10 N/mm produced the best fit with experimental observations. These results indicate that tensile strength and fracture energy are closely linked and collectively govern the non-linear response of CBM walls.

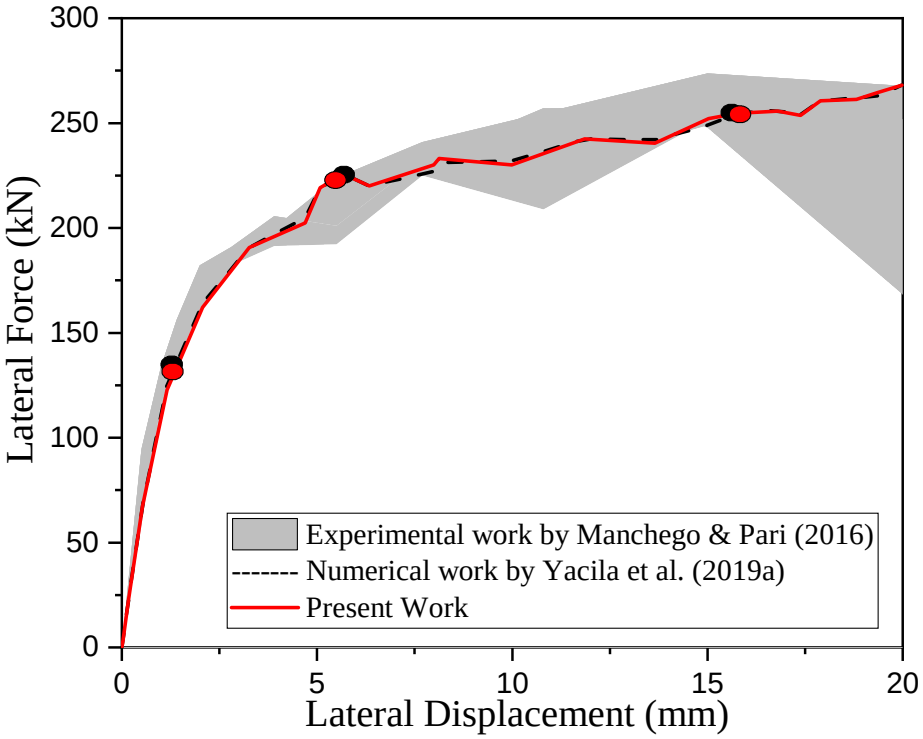

Figure 3.12: Comparison of pushover curves obtained in present work with Yacila et. al. [72]

3.5 Validation

Yacila et al. [72] conducted a thorough comparison between the results from pushover analysis and the experimental test results provided by Machengo and Pari [103]. The primary focus of this work was to examine the envelope curve specifically in the direction of the lateral push. The envelope curve is crucial because it represents the maximum response of the structure under increasing lateral loads, highlighting critical performance levels.

As illustrated in Figure 3.12, the pushover curve obtained from the numerical modelling carried out in the present study closely aligns with the pushover curve reported by Jhair et al. [72] at significant performance levels. These levels include: (1) the end of linear behaviour, where the structure responds elastically and returns to its original shape upon unloading; (2) the beginning of yielding, which marks the point where the structural system starts to experience permanent deformations; and (3) the ultimate strength capacity, indicating the maximum load that the structure can withstand before failure.

Table 3.3 shows the values for lateral force and lateral displacement obtained at the end of

Table 3.3: Comparison of lateral displacement and lateral force

Model	**Lateral Disp.** (mm)	**Lateral Force** (kN)
Yacila et al. [72]	1.20805	128.4
Present Work	1.20805	128.7
Yacila et al. [72]	5.68233	226.7
Present Work	5.672334	226.4
Yacila et al. [72]	15.00	252.1
Present Work	15.034	252.1

linear behaviour, at the onset of yielding, and at the ultimate load capacity for the numerical work done by Yacila et al. [72] and the present work. The discrepancies between our numerical results and those of Yacila et al. [72] are minimal: a zero percent error in lateral displacement and a 0.23% error in lateral force at the end of linear behaviour, a 0.17% error in displacement and a 0.13% error in force at the onset of yielding, and a 0.22% error in displacement and a zero percent error in force at the ultimate strength capacity.

This close agreement, between the pushover curves from the current study with that of Yacila et al. [72], confirms the validity and accuracy of the ABAQUS simulation results used in the present research. The ability to replicate these key performance points demonstrates that the numerical model is a reliable tool for predicting the structural behaviour under lateral loads.

Furthermore, Figure 3.13 provides a visual comparison of the cracking patterns observed in the model presented by Yacila et al. [72] and the present study. Cracking patterns are a critical aspect of structural analysis as they reveal how the structure distributes and handles stress under loading conditions. The similarities in the observed cracking patterns further validate the numerical model used in the current study, indicating that it can accurately replicate not only the overall load-bearing behaviour but also the detailed failure mechanisms of the structure.

In summary, the present study's numerical modelling results have been successfully validated against both the pushover analysis results of Yacila et al. [72] and the experimental observations by Machengo and Pari [103]. This validation is evidenced by the strong agreement in the pushover curves at various performance levels and the comparable cracking patterns.

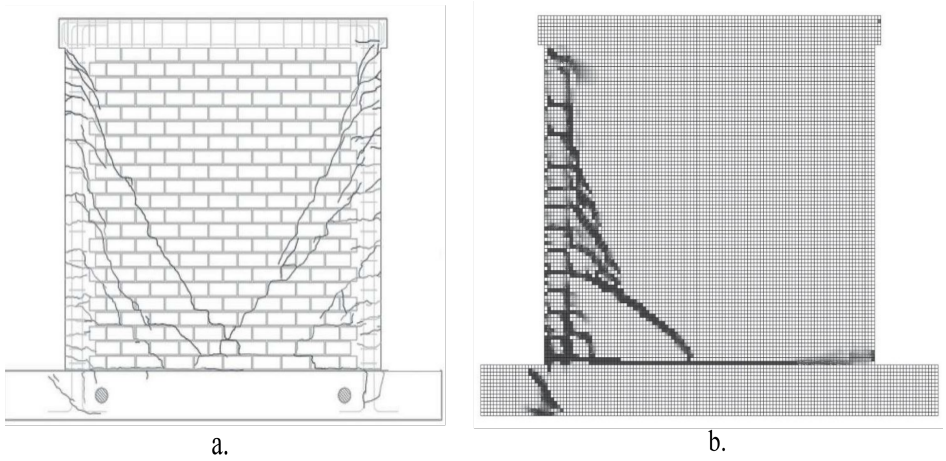

a. b.

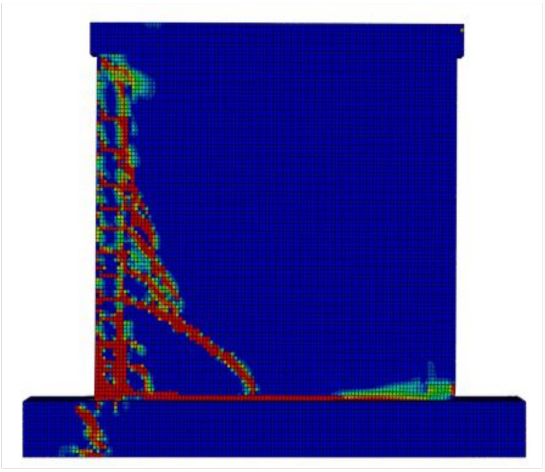

c.

Figure 3.13: Comparing damage pattern a. model by Manchego & Pari [103], b. model by Yacila et al. [72], c. present work

Consequently, the ABAQUS simulation approach employed in this research is confirmed to be a reliable and accurate method for analysing structural behaviour under lateral loads.